European Journal of Medical Research

RESEARCH

Open Access

Identification of diagnostic biomarkers and immune cell infiltration in tongue squamous cell carcinoma using bioinformatic approaches

Meng Shi[1†], Huixin Dou[1†], Xinzhe Lou[1], Wenting Jiang[2], Hao Wang[1*] and Yingying Su[1*]

Abstract

Objective In this study, we employed a bioinformatics approach to identify diagnostic biomarkers for tongue squamous cell carcinoma (TSCC) and investigate the infiltration of immune cells in TSCC, as well as the relationship between biomarkers and immune cells.

Methods We obtained the TSCC expression dataset from a database and conducted differential gene expression analysis between TSCC and adjacent normal tissues using R software. Enrichment analysis of the differentially expressed genes (DEGs) was performed using the DAVID website. Protein interaction networks for the DEGs were constructed, and hub genes were identified using tools such as STRING and Cytoscape. Survival analysis was conducted to identify diagnostic biomarkers and the infiltration of immune cells in TSCC was analyzed using the inverse convolution algorithm with Cibersort software. Finally, the expression of the discovered molecules was verified through clinical pathological sections.

Results We identified 24 DEGs in TSCC, primarily associated with signal transduction, substance metabolism, innate immune response, and other related signaling pathways. Among the 24 hub genes screened through the construction of a protein–protein interaction (PPI) network, seven (MMP13, POSTN, MMP9, MMP10, MMP3, SPP1, MMP1) exhibited prognostic value. Survival analysis indicated that SPP1 demonstrated diagnostic potential. The expression level of the SPP1 gene showed a correlation with TSCC as well as several immune cell types, including macrophage M0, M1, M2, $CD8^+$ T cell, activated NK cell, and monocyte ($p < 0.05$). Histological results confirmed higher expression of SPP1 in TSCC tissues compared to adjacent non-cancerous tissues, particularly in CD68-expressing macrophages.

Conclusion Our findings suggest that SPP1 serves as a diagnostic biomarker for TSCC and is involved in immune cell infiltration within TSCC tissues. The correlation between SPP1 and macrophages may offer new insights for targeted therapeutic research on TSCC.

Keywords Tongue squamous cell carcinoma, Bioinformatic approach, Biomarkers, Immune cells, SPP1, Macrophages

†Meng Shi and Huixin Dou have contributed equally to this work.

*Correspondence:
Hao Wang
13701131933@139.com
Yingying Su
reliayysu@163.com
Full list of author information is available at the end of the article

Introduction

Oral squamous cell carcinoma (OSCC) is a highly prevalent malignancy, with an annual global incidence of 405,000 new cases reported [22]. OSCC is commonly associated with risk factors such as tobacco use, excessive alcohol consumption, and human papillomavirus (HPV) infection [8]. Among the subtypes of OSCC, tongue squamous cell carcinoma (TSCC) is the most common, accounting for 80% of all OSCC cases. TSCC is characterized by aggressive features, a high incidence of recurrence and metastasis, and a poor prognosis [5, 16]. Despite advancements in diagnosis and treatment, the 5-year survival rate for TSCC remains around 50%, and it can severely impact patients' quality of life by restricting tongue movement, causing difficulty in eating and swallowing, and posing a significant threat to human health [8, 25].

The standard treatment for TSCC typically involves surgical resection, with adjuvant therapies such as chemotherapy and radiotherapy [26]. However, these modalities often have substantial adverse effects, and approximately one-third of patients face the risk of recurrence and developing resistance to chemotherapy and radiotherapy [6]. Hence, there is an urgent need to identify novel targets for TSCC treatment and develop more effective drugs and approaches. Advancements in molecular profiling technology have facilitated faster and easier DNA/RNA sequencing and protein detection. Bioinformatics methods can be utilized to identify differentially expressed genes (DEGs) or proteins between tumors and normal tissues.

Recent studies have emphasized the correlation between tumors and the immune system, as the degree of immune cell infiltration within tumors is closely related to tumor growth, progression, and patient outcomes [34]. The tumor microenvironment comprises diverse types of immune cells, including T lymphocytes, B lymphocytes, tumor-associated macrophages, dendritic cells, and natural killer cells [1]. The type and extent of immune cell infiltration in solid tumor tissue are closely associated with the clinical characteristics of these tumors, and immune cell infiltration can be used for tumor risk classification [15, 18, 44]. Some biomarkers with altered levels in cancer tissues may influence tumor development by interacting with immune cells. However, only a limited number of TSCC prognostic biomarkers have been investigated from an immunological perspective. Therefore, it is crucial to elucidate the association between local immune activity and TSCC and explore the relationship between TSCC biomarkers and immune cells.

In our research, we downloaded TSCC mRNA expression data from databases and employed bioinformatics techniques to screen and analyze differentially expressed genes in TSCC. Additionally, we utilized the Cibersort algorithm to calculate the infiltration levels of various immune cell types in TSCC. This allowed us to explore the correlation between TSCC biomarkers and relevant immune cells. Our findings were preliminarily validated using histological methods, providing new insights for targeted therapeutic research on TSCC.

Materials and methods

Data access

We accessed the NCBI-GEO (Gene Expression Omnibus) database (https://www.ncbi.nlm.nih.gov/geo), which provides a collection of microarray/gene profiles and NGS data. For our study, we selected three datasets (GSE31056, GSE34105, and GSE13601) that contained expression profiles of tongue squamous cell carcinoma (TSCC) samples [4, 32, 33]. To ensure accuracy, we only included samples from the database that clearly indicated the sampling location as the tongue. The GSE31056 dataset consisted of 16 TSCC and 17 normal tissue samples. In the GSE34105 dataset, we filtered out 62 TSCC and 16 normal tissue samples. Lastly, the GSE13601 dataset provided us with a total of 30 TSCC and 25 normal tissue samples.

Identification of DEGs

We utilized the Limma package in R to identify DEGs between TSCC samples and normal tissues, considering an adjusted p-value < 0.05 and $|\log2FC| > 2$ as the criteria. In the Limma analysis, we used the default parameter. Since false positives sometimes occur when multiple comparisons are made which could lead us to incorrectly reject the true null hypothesis, we need to control the false discovery rate using a multiple comparison correction method to ensure that the overall false positive rate does not exceed the preset threshold. We, therefore, used the Benjamini–Hochberg (BH) method to calculate adjusted p-values to decrease the false discovery rate. In many biological studies, a two-fold change is often considered to be biologically meaningful as it may correspond to significant alterations in gene expression or protein abundance. The log2 transformation provides a more intuitive representation of these multiplicative changes. Additionally, selecting this threshold is a balance between sensitivity and specificity. A lower threshold might increase the chances of detecting true biological changes but also risks increasing false positives. Conversely, a higher threshold might reduce false positives but could also overlook important changes. The fold change represents the expression level in TSCC tissue samples relative to normal tissue

samples. Subsequently, we visualized the DEGs using SANGERBOX (http://sangerbox.com/Index), FUNRICH, and R. To obtain the common DEGs across all three datasets, we constructed a Venn diagram.

GO and KEGG enrichment analysis

To explore the biological functions of the DEGs, we performed Gene Ontology (GO) annotation and Kyoto Encyclopedia of Genes and Genomes (KEGG) pathway enrichment analyses using the DAVID website (https://david.ncifcrf.gov/home.jsp). We considered a cutoff of $p < 0.05$ and FDR < 0.05 for significance. The GO enrichment analysis included biological processes (BP), molecular functions (MF), and cellular components (CC) [11].

Construction of PPI network and selection of hub genes

We constructed the PPI network using the STRING database https://string-db.org/) [35]. The network was visualized using Cytoscape software (version 3.9.1), and the top 20 genes were selected as hub genes using the cytoHubba plug-in [2]. The default parameters for hub gene selection were as follows: degree cutoff = 10, k-core = 2, node score cutoff = 0.2, and max. depth = 100.

Clinical prognostic model analysis

We downloaded RNA-sequencing expression profiles and corresponding clinical information for TSCC from the TCGA dataset (https://portal.gdc.cancer.gov). Univariate and multivariate Cox regression analyses were performed to identify the appropriate terms for building a nomogram. The "forestplot" R package was used to display the *p*-value, hazard ratio (HR), and 95% confidence interval (CI) for each variable.

Systematic analysis of immune infiltrates

To gain a comprehensive understanding of the immune microenvironment in TSCC tissues and identify distinct immune cell proportions, we employed CIBERSORT (https://cibersort.stanford.edu/) to normalize and process the raw RNA-seq read counts. CIBERSORT utilizes a deconvolution model based on a presumed linear connection between mixed expression profiles in tissue samples and isolated cell type expression profiles to estimate the relative percentage of main immune cell types. We downloaded RNA-sequencing expression profiles and corresponding clinical information for TSCC from the TCGA dataset. Unless otherwise specified, two-group data were analyzed using the Wilcoxon test, and *p*-values less than 0.05 were considered statistically significant ($^{*}p < 0.05$).

Immunohistochemistry and immunofluorescence staining

We obtained paraffin sections of TSCC and healthy paracancerous tissue for immunohistochemistry and immunofluorescence staining. The research was conducted in accordance with the standards set by the Declaration of Helsinki and was authorized by the Ethics Committee of Beijing Stomatological Hospital Affiliated with Capital Medical University (approval number: CMUSH-IRB-KJ-PJ-2022-26). Written informed consent was obtained from all participants.

The following steps were performed for immunohistochemistry staining: after deparaffinization and rehydration, antigen retrieval was conducted using TE (Tris and ethylenediaminetetraacetic acid) buffer at pH 9.0. Sections were then blocked for endogenous peroxidase using hydrogen peroxide in methanol, followed by treatment with 10% normal goat serum and 0.1% Triton X-100. The tissues were incubated overnight at room temperature with a rabbit anti-SPP1 antibody (1:50, Proteintech, 22952-1-AP). Subsequently, the sections were incubated with biotinylated anti-rabbit IgG secondary antibodies (ZSGB-Bio) and visualized using 3,3′-diaminobenzidine (DAB) at room temperature. Brief counterstaining with H&E staining was performed, and the sections were mounted with neutral gum. Analysis of the stained sections was carried out using a Zeiss AxioPlan microscope.

For immunofluorescence staining, the sections were blocked with a 10% goat serum solution for 30 min at room temperature. They were then incubated overnight at 4 °C with primary antibodies against SPP1 (1:50, Proteintech, 22952-1-AP) and CD68 (1:100, Invitrogen, 14-0688-82). After washing the tissue sections three times in PBS (pH 7.2), secondary antibodies, such as goat anti-rabbit conjugated with Alexa Fluor 594 and goat anti-mouse conjugated with Alexa Fluor 488 (ZSGB-Bio), were applied for 1 h at 37 °C. Subsequently, the tissue sections were washed five times in PBS (pH 7.2), and DAPI (Sigma-Aldrich) was used for nuclear staining for 20 min at 37 °C. Coverslips were mounted in a Fluorescence Mounting Medium (Dako, Glostrup, Denmark) for visualization.

Results

Screening and identification of DEGs

We screened microarray datasets from the NCBI-GEO database to identify DEGs in TSCC tissue samples. The datasets used were GSE31056, GSE34105, and GSE13601. From GSE31056, which is based on the GPL10526 platform, we selected 16 TSCC and 17 normal tissue samples. GSE34105, based on the GPL14951 platform, provided data from 62 TSCC and 16 normal tissue samples. Lastly, GSE13601, based on the GPL8300 platform, included 30 TSCC and 25 normal tissue samples. R software was utilized to screen for

DEGs, with adjusted $p<0.05$ and $|\log_2 FC|>2$ as the cut-off criteria. Ultimately, we extracted 862, 413, and 399 DEGs from these three datasets, respectively (Fig. 1A–C). Additionally, using R software, we performed cluster analysis and generated a heatmap to visualize the expression of 24 DEGs from the three datasets (Fig. 1D–F). Through FUNRICH software, we identified 24 consistent DEGs across all three genome datasets (Fig. 1G). These DEGs consisted of 5 downregulated genes and 19 upregulated genes (Table 1 and Fig. 1H, I).

Gene ontology (GO) and signaling pathway enrichment analyses

The selected candidate DEGs were subjected to Gene Ontology (GO) analysis using the Database for Annotation, Visualization, and Integrated Discovery (DAVID). The DEGs were divided into three functional groups: molecular functional group, biological process group, and cell component group. In the biological process group (Fig. 2A), the DEGs were enriched in processes such as collagen catabolic process, extracellular matrix disassembly, extracellular matrix

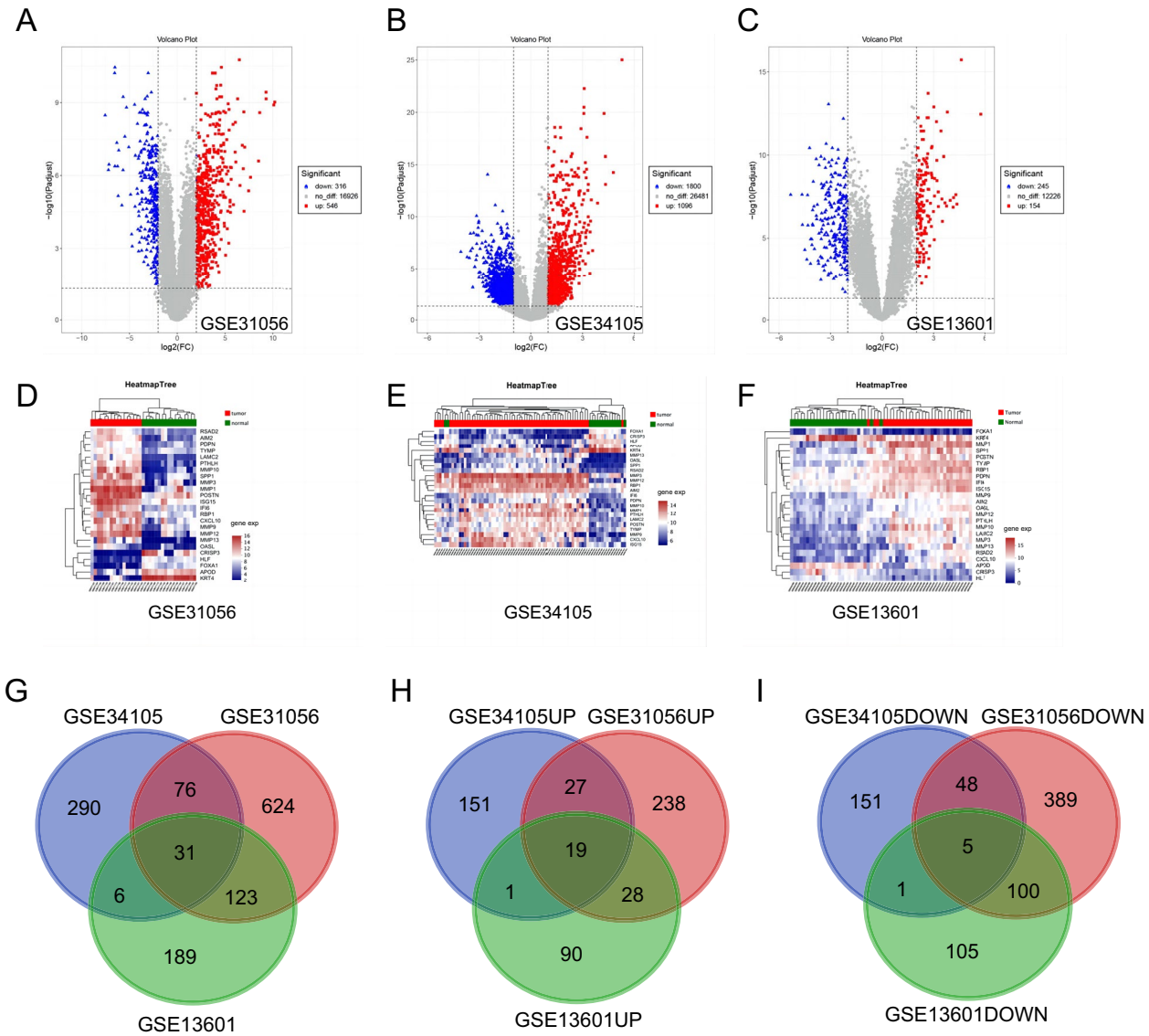

Fig. 1 Screening and Identification of DEGs. A total of 24 DEGs were indentified. (**A**-**C**) Distributions of DEGs in tumor and control tissues in the database of GSE31056 (**A**), GSE34105 (**B**), and GSE13601 (**C**) were displayed in the volcano maps (|log2FC| >2 and adjusted *p*-value < 0.05). Red dots stand for up-regulated genes, blue dots stand for down-regulated genes and grey dots stand for normal expression in volcanoes. Each dot represents a gene. (**D**-**F**) The heatmaps showed the relative expression levels of DEGs between normal and tumor samples in the database of GSE31056 (**D**), GSE34105 (**E**), and GSE13601 (**F**). Each row represents a gene and each column represents a sample. The colour and intensity of the boxes represent changes of gene expression. From dark red to dark blue, the expression of genes decreased. (**G**–**I**) Venn diagram was visualized in FUNRICH software

Table 1 Up and down regulation of 24 differentially expressed genes (DEGs)

DEGs	Gene symbol						
Up	PDPN	POSTN	TYMP	IFI6	CXCL10	LAMC2	MMP1
	MMP9	MMP10	MMP12	MMP13	PTHLH	RBP1	SPP1
	OASL	RSAD2	ISG15	MMP3	MMP9	AIM2	
Down	CRISP3	HLF	FOXA1	APOD	KRT4		

organization, response to beta-amyloid and proteolysis, and innate immune response. The molecular function group (Fig. 2B) showed enrichment in processes like metalloendopeptidase activity, serine-type endopeptidase activity, endopeptidase activity, zinc ion binding, collagen binding, and peptidase activity. The cell component group (Fig. 2C) indicated enrichment in processes associated with the extracellular matrix, extracellular space, and extracellular region. Furthermore, our analysis revealed common signaling pathways and reaction processes among the candidate DEGs (Fig. 2D). These DEGs were found to be involved in pathways such as the IL-17 signaling pathway, TNF signaling pathway, relaxin signaling pathway, lipid metabolism, and atherosclerosis.

PPI network screening and analysis

We used the STRING database to filter the 24 DEGs and construct a PPI network consisting of 24 nodes and 51 edges (Fig. 2E). The average node degree was 4.25, and the average local clustering coefficient was 0.612. The PPI concentration p-value was found to be less than 1.0e−16. Among the DEGs, PDPN, RBP1, HLF, and APOD did not connect within the PPI network, resulting in the identification of 20 key genes. We performed a k-means clustering analysis to categorize the DEGs into three groups. Subsequently, we used CYTOSCAPE to remove genes without nodes and create a PPI network diagram based on the interaction and expression between the nodes (Fig. 2F). Further applying the MCODE modular analysis in CYTOSCAPE, we screened out 7 candidate genes (Table 2). Additionally, we sought to validate the results using an alternative calculation. We employed cytoHubba, a Cytoscape plugin, to perform topological analysis methods and rank the nodes in the PPI network. Four centrality indexes, including maximal clique centrality (MCC), maximum neighborhood component (MNC), edge percolated component (EPC), and degree, were chosen to filter the top 20 genes. All 7 previously screened genes ranked highly (Table 3).

Prognostic analysis

We downloaded RNA-sequencing expression profiles and corresponding clinical information for TSCC from the TCGA dataset, including a total of 156 patients. Univariate and multivariate Cox regression analysis was conducted to identify 24 DEGs and construct a predictive signature in the discovery group (Fig. 3A, B). The results of the analysis indicated that only one DEG, SPP1, was considered a prognostic factor ($p < 0.05$). Furthermore, the combined Kaplan–Meier curves with the log-rank p-test demonstrated a clear association between SPP1 and overall survival in TSCC (Fig. 3C).

Analysis of SPP1 gene expression and immune cell infiltration in TSCC tissue

To evaluate the relative abundance of major immune cell subsets, we employed CIBERSORT, which revealed varying proportions of activated monocytes and macrophages in TSCC (Fig. 4A). A comparison of immune cell infiltration in normal and TSCC tissues revealed significant differences, with a higher number of immune cells, including M0 and M1 macrophages, and T cell regulatory (Tregs), observed in TSCC tissues. Conversely, the control group exhibited higher recruitment of monocytes, M2 macrophages, naïve B cells, $CD8^+$ T cells, $CD4^+$ T cell memory resting, myeloid dendritic cells at rest, and activated mast cells. Additionally, CIBERSORT analysis was used to examine the relationship between SPP1 gene expression and immune cell infiltration in TSCC samples from the TCGA database (Fig. 4B). TSCC samples with high SPP1 gene expression displayed higher distributions of M0 and M2 macrophages, while samples with low SPP1 gene expression exhibited elevated levels of naïve B cells, $CD8^+$ T cells, T cell follicular helper cells, activated NK cells, monocytes, M1 macrophages, and neutrophils.

Prognostic gene validation using clinical tissue samples

To validate the prognostic significance of the identified gene SPP1, immunohistochemical (IHC) staining was performed on para-cancer tissues and tumor tissues. The results confirmed that SPP1 was highly expressed in TSCC tissues compared to para-cancer tissues (Fig. 5A), aligning with the conclusions drawn from the research. Furthermore, double immunolabeling demonstrated that the increased expression of SPP1 in tumor tissues was primarily localized to macrophages expressing CD68 (Fig. 5B), suggesting that the production of SPP1

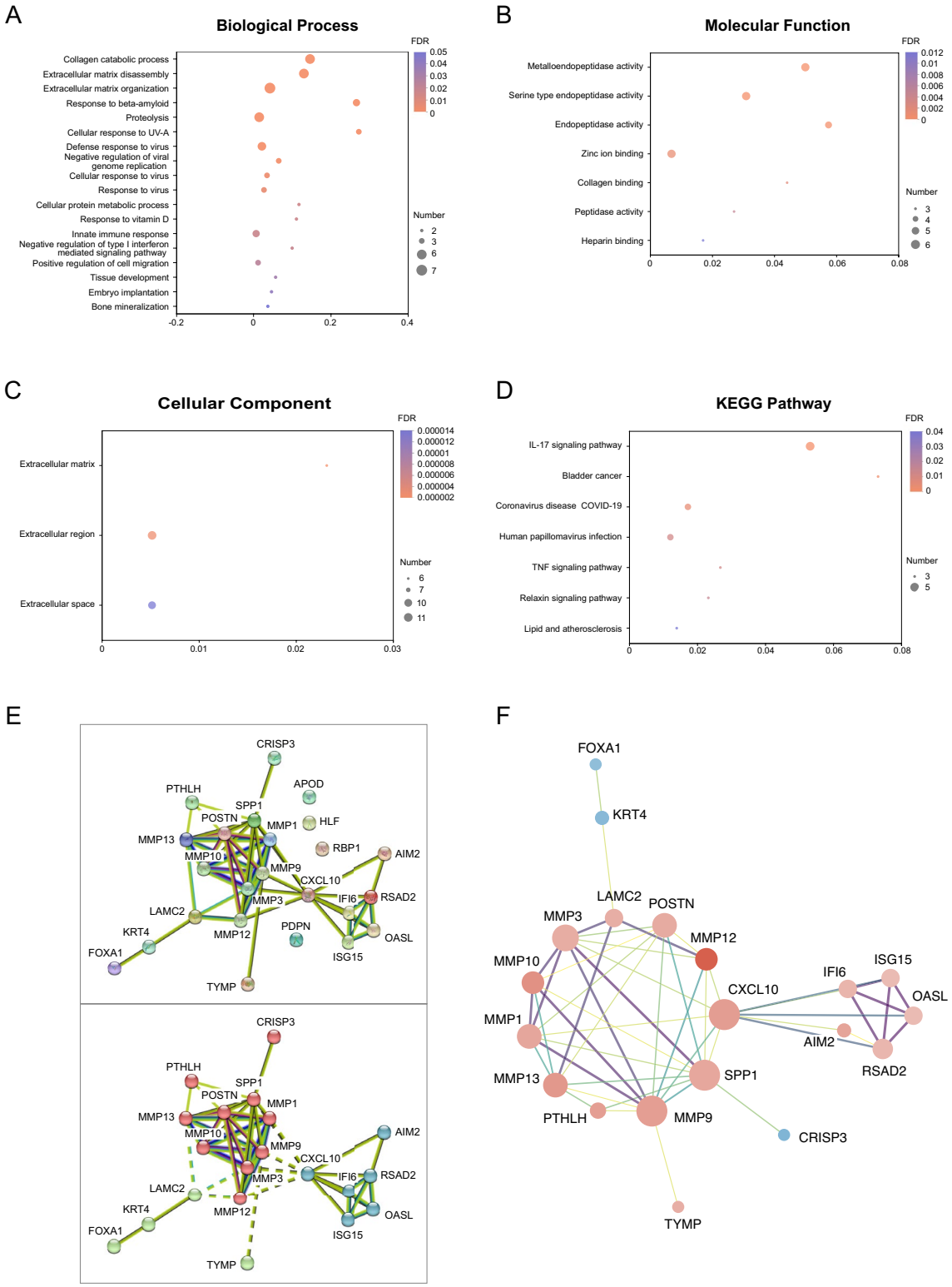

Fig. 2 Enrichment Analyses and PPI network analysis. The enrichment analysis of 24 DEGs in tumor (David 6.8). (**A**–**C**) Bubble diagram of GO enrichment in biological process terms, molecular function terms and cellular component terms. (**D**) Bubble diagram of KEGG enriched terms. (**E**) The PPI network was visualized in STRING that contained 24 nodes and 51 edges, with an average node degree of 4.25, and an average local clustering coefficient of 0.612 with a PPI concentration *p*-value less than 1.0e-16. (**F**, **G**) Four out of 24 DEGs (PDPN, RBP1, HLF, and APOD) did not fall within the PPI network

Table 2 Seven DEGs in MCODE modular analysis

DEGs	Gene symbol						
Up	MMP13	POSTN	MMP9	MMP10	MMP3	SPP1	MMP1

Table 3 Comparison of hub genes ranked in the cytohubba plugin of cytoscape

Catalog	Rank methods in cytoHubba			
	MCC	MNC	Degree	EPC
Gene top 20	**SPP1**	**SPP1**	CXCL10	**SPP1**
	MMP9	**MMP9**	**SPP1**	**MMP9**
	POSTN	**MMP3**	**MMP9**	CXCL10
	MMP1	**POSTN**	**MMP3**	**MMP3**
	MMP10	**MMP1**	**MMP13**	**POSTN**
	MMP3	**MMP13**	**POSTN**	**MMP1**
	MMP13	**MMP10**	**MMP1**	**MMP13**
	CXCL10	MMP12	**MMP10**	**MMP10**
	MMP12	CXCL10	MMP12	MMP12
	RSAD2	RSAD2	RSAD2	LAMC2
	OASL	OASL	LAMC2	PTHLH
	IFI6	IFI6	OASL	RSAD2
	ISG15	ISG15	IFI6	IFI6
	PTHLH	PTHLH	ISG15	ISG15
	LAMC2	LAMC2	PTHLH	OASL
	AIM2	AIM2	AIM2	AIM2
	KRT4	CRISP3	KRT4	CRISP3
	CRISP3	TYMP	CRISP3	TYMP
	TYMP	FOXA1	TYMP	KRT4
	FOXA1	KRT4	FOXA1	FOXA1

The bolded genes represent the overlapping hub genes that were also screened out by using MCODE modular analysis in CYTOSCAPE

MCC maximum clique centrality, *MNC* maximum neighborhood component, *degree* degree of connection between nodes, *EPC* edge percolated component

is associated with macrophages. This finding further supports the involvement of SPP1 and its interaction with macrophages in tongue squamous cell carcinoma.

Discussion

In this study, we aimed to identify potential therapeutic targets and develop more effective approaches for the treatment of TSCC. By analyzing mRNA expression profiles and immune cell infiltration in TSCC, a total of 24 DEGs related to TSCC were identified. By constructing a PPI network and performing enrichment analysis, seven key genes were screened, including MMP13, POSTN, MMP9, MMP10, MMP3, SPP1, and MMP1. Among them, SPP1 was found to have prognostic value for TSCC. Secretory phosphoprotein 1 (SPP1), also known as osteopontin (OPN) or early T lymphocyte activation 1 protein, is a multifunctional secretory acidic glycoprotein involved in various physiological and pathological processes [3]. While healthy organisms only secrete small amounts of SPP1 for normal physiological functions, its overexpression has been observed in numerous human tumors, including lung, prostate, breast, colorectal, and liver cancers [30]. High levels of SPP1 expression in tumor tissues have been associated with poorer patient prognosis, indicating its potential as a biomarker for monitoring tumor progression [13, 19, 20, 31, 41].

Previous studies have linked SPP1 expression to various aspects of tumorigenesis and tumor progression, such as angiogenesis [14], distant metastasis [17, 23, 29], maintenance of tumor cell stemness [24], and activation of cell proliferation pathways [12, 28]. In the context of oral squamous cell carcinoma (OSCC), several studies have suggested that SPP1 may play a role in its occurrence and development [9, 10, 42, 46]. In the present study, SPP1 expression was found to be significantly elevated in TSCC tissues compared to normal tissues, consistent with previous findings by other researchers [38]. Moreover, the expression levels of SPP1 were found to significantly correlate with patients' survival compared to other differentially expressed genes (DEGs). These findings highlight the potential of SPP1 as a molecular therapeutic target in TSCC.

The tumor microenvironment (TME) is composed of various cell populations that play critical roles in tumor pathogenesis. Among the immune cells infiltrating tumors, macrophages are the major cell type involved and serve as a key link between inflammation and cancer. Macrophages can be polarized into two distinct phenotypes: M1 and M2 [36]. M1 macrophages are associated with cytokine production, recruitment of pro-immune stimulated leukocytes, and phagocytosis of tumor cells, while M2 macrophages promote tumor development through basement membrane rupture, leukocyte recruitment, angiogenesis, and immune evasion. Higher levels of M1 macrophages have been associated with better patient prognosis, while higher levels of M2 macrophages have been linked to worse prognosis in various tumor types [21, 40]. Therefore, the balance between M1 and M2 macrophages in the tumor microenvironment can influence clinical outcomes. Understanding the composition and functional characteristics of immune cell infiltration, particularly macrophages, provides valuable insights into tumor biology and potential therapeutic targets. In this study, the increased expression of SPP1 was found

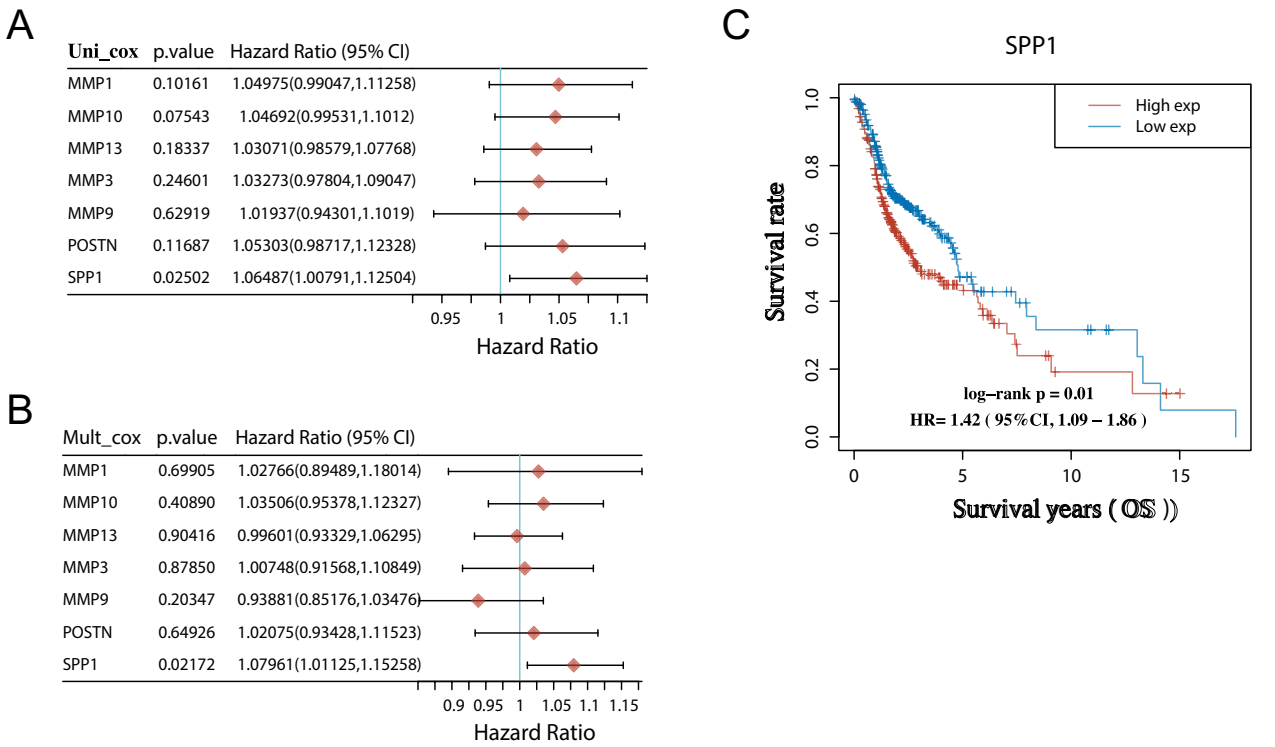

Fig. 3 Prognostic model analysis. (**A**, **B**) The p value, risk coefficient (HR) and confidence interval are analyzed by univariate and multivariate Cox regression. (**C**) Kaplan-Meier survival analysis of the SPP1 gene signature from TCGA dataset, comparison among was made by log-rank test

to be localized mainly to CD68-expressing macrophages, indicating that macrophages are associated with the production of SPP1 in TSCC. Previous studies have shown that SPP1 can influence macrophage behavior and polarization in different cancer models. For example, in a hepatocellular cancer model, SPP1 produced by tumor cells was found to activate the PI3K-AKT-p65 signaling pathway, leading to the secretion of colony-stimulating factor 1 by macrophages, resulting in macrophage infiltration and M2 polarization [45]. Similarly, in a glioblastoma model, SPP1 was found to promote macrophage migration and preserve the properties and phenotype of M2 macrophages through binding to integrin avβ5 receptors. The expression levels of SPP1 were also found to be associated with the degree of macrophage infiltration and glioma grade in patients, suggesting that the interaction between SPP1 and macrophages affects immunological regulation and tumor progression [37].

In our study, using the "deconvolution algorithm," we analyzed immune cell infiltration in paraneoplastic tissues and tongue carcinoma tissues and observed significant differences in the immune cell composition between the two. CIBERSORT calculates based on gene expression profile data, which can classify and identify mixed cell types, and can help researchers better understand the gene expression profile data and dig deeper into the background biological information, which is of great significance in future research. The parameter adjustment in CIBERSORT is mainly permutation, which refers to the number of times of alignment on the analysis, and the larger the number, the more accurate the final result will be. Elevated SPP1 expression was associated with a higher prevalence of M2 macrophages during immune cell infiltration analysis. Previous studies have demonstrated that M2 macrophages can play a role in promoting tumor cell proliferation and suppressing lymphatic T cell function through the release of various cytokines. They have been identified as important factors influencing host immunity and promoting immune evasion by tumor cells [27]. While several studies have explored the impact of SPP1 expression on tongue tumor cells, there is relatively less research on the involvement of SPP1-affected macrophages in TSCC.

In the past several years, compelling evidence has demonstrated that the posttranscriptional regulation of mRNA, such as N^6-methyladenosine (m^6A) RNA methylation, plays a critical role in controlling RNA metabolism and function in tumor immune response [7, 39]. A recent study has revealed that m6A modification plays a crucial role in the diversity and complexity of the immune microenvironment of periodontitis [43]. Understanding the role of posttranscriptional regulation of mRNA in

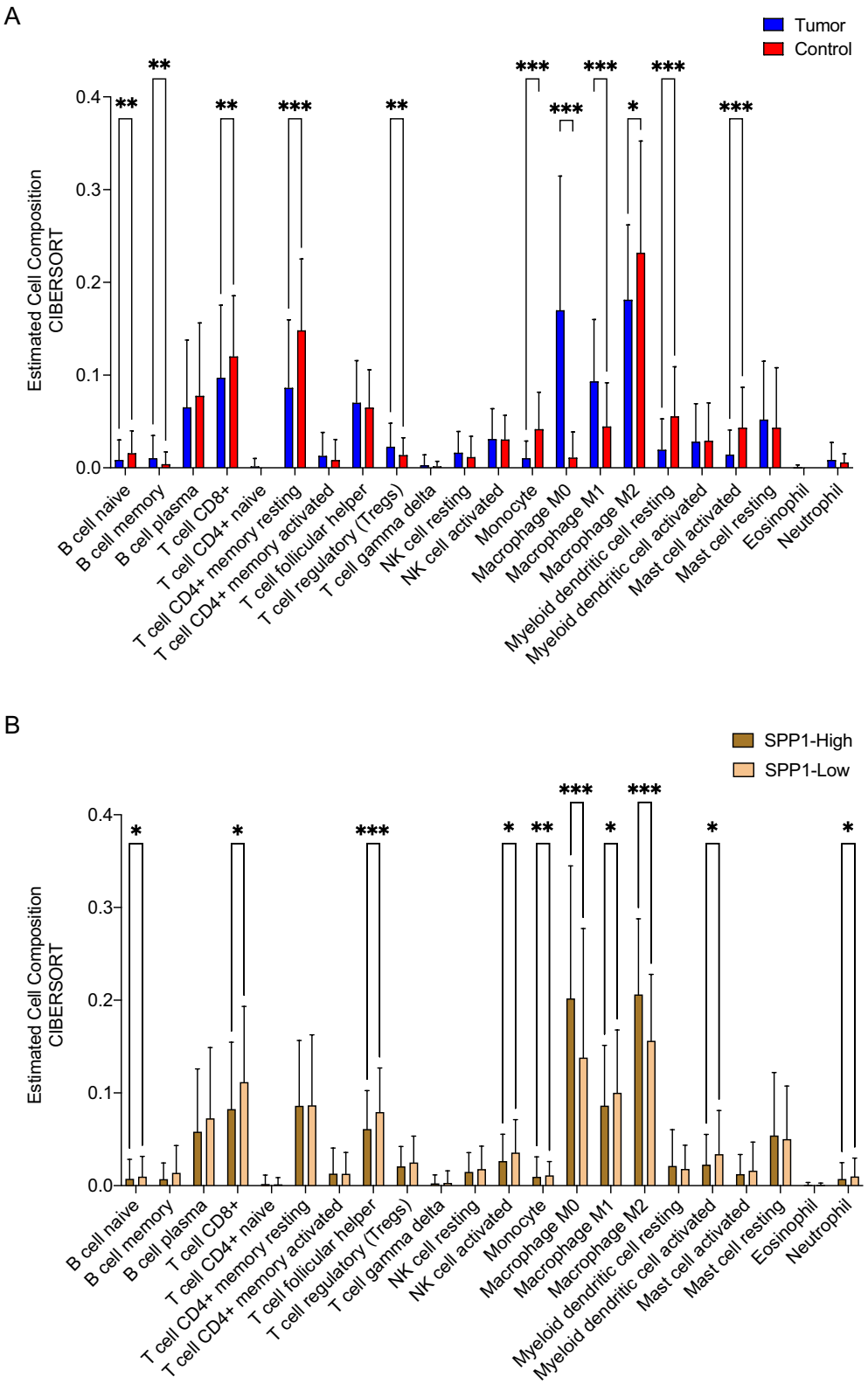

Fig. 4 Analysis of SPP1 gene expression and immune cell infiltration in TSCC tissue. (**A**) The percentage of immune cells in TSCC and normal tissues. Blue represents TSCC sample, red represents normal tissue sample; horizontal coordinates indicate immune cells, vertical coordinates indicate percentage of immune cells. (**B**)Relationship between SPP1 gene expression and immune cell infiltration in TSCC tissues

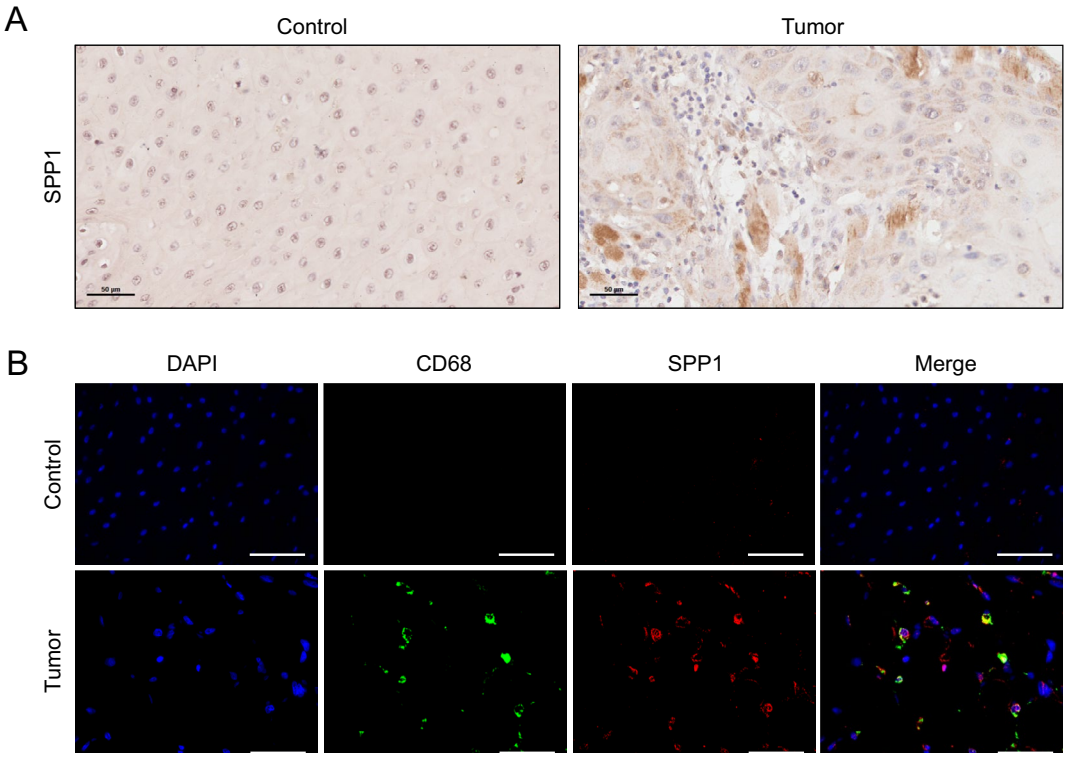

Fig. 5 SPP1 was highly expressed in tongue from patients with TSCC. (**A**) Immunohistochemical staining of SPP1 in cancerous and paracancer tissues of the tongue. (**B**) Representative immunofluorescence images of SPP1 (red) and CD68 (green) from cancerous and paracancer tissues of the tongue (Scale bars, 20 μm)

TSCC pathogenesis and immune response could provide a promising therapy for TSCC.

This study, however, is subjected to some limitations that could be addressed in future research. First, the expression of SPP1 in TSCC was found to be correlated with the expression of macrophage marker on our study. To improve further upon these findings, we are now collaborating with other institutions to enroll additional patients to carry out external validation of the expression of SPP1 and other immunological biomarkers in TSCC. Second, the molecular mechanism regulating SPP1 expression and immune microenvironment in TSCC is unclear. In the past several years, compelling evidence has demonstrated that the posttranscriptional regulation of mRNA, such as N^6-methyladenosine (m^6A) RNA methylation, plays a critical role in controlling RNA metabolism and function in tumor immune response [7, 39]. A recent study has revealed that m6A modification plays a crucial role in the diversity and complexity of the immune microenvironment of periodontitis [43]. Understanding the role of posttranscriptional regulation of mRNA in TSCC pathogenesis and immune response could provide a promising therapy for TSCC. Further study may focus on the potential roles of mRNA modification in TSCC immunity and therapy.

Based on the findings of our analysis, the interaction between SPP1 and macrophages could represent a potential immune-related therapeutic target in TSCC. Further research into the role of SPP1 in modulating macrophage behavior and its impact on the immune response in TSCC may uncover novel therapeutic strategies for the disease.

Acknowledgements
Not applicable.

Declaration of generative AI and AI-assisted technologies in the writing process
During the preparation of this work the authors used ChatGPT in order to improve readability. After using this tool, the authors reviewed and edited the content as needed and took full responsibility for the content of the publication.

Author contributions
Y.S. and H.W. conceived and designed the study and revised the manuscript. M.S. and H.D. analysed most of the data, and wrote the initial draft of the paper. X.L. and W.J. helped perform the analysis with constructive discussions. All authors read and approved the final manuscript.

Funding
This research did not receive any specific grant from funding agencies in the public, commercial, or not-for-profit sectors.

Availability of data and materials
Sequence data that support the findings of this study have been deposited in the NCBI-GEO (Gene Expression Omnibus) database, the datasets number are GSE31056, GSE34105, and GSE13601.

Declarations

Ethics approval and consent to participate
The studies involving human participants were reviewed and approved by the Ethics Committee of Beijing Stomatological Hospital Affiliated to Capital Medical University. The patients/participants provided their written informed consent to participate in this study.

Consent for publication
Not applicable.

Competing interests
The authors declare no competing interests.

Author details
[1]Department of Stomatology, Beijing Tiantan Hospital, Capital Medical University, No. 119 South Fourth Ring West Road, Fengtai District, Beijing 100070, People's Republic of China. [2]Department of Periodontology, Fujian Key Laboratory of Oral Diseases, Fujian Provincial Engineering Research Center of Oral Biomaterial, School and Hospital of Stomatology, Fujian Medical University, Fuzhou 350004, Fujian, China.

Received: 10 January 2024 Accepted: 23 July 2024
Published online: 21 August 2024

References

1. Birbrair A. Tumor microenvironments in organs: from the brain to the skin—part B. In: Advances in experimental medicine and biology. Cham: Springer International Publishing; 2020. https://doi.org/10.1007/978-3-030-59038-3.
2. Chin C-H, Chen S-H, Wu H-H, et al. CytoHubba: identifying hub objects and sub-networks from complex interactome. BMC Syst Biol. 2014;8(S4):S11. https://doi.org/10.1186/1752-0509-8-S4-S11.
3. Clemente N, Raineri D, Cappellano G, et al. Osteopontin bridging innate and adaptive immunity in autoimmune diseases. J Immunol Res. 2016;2016:1–15. https://doi.org/10.1155/2016/7675437.
4. Estilo CL, O-charoenrat P, Talbot S, et al. Oral tongue cancer gene expression profiling: identification of novel potential prognosticators by oligonucleotide microarray analysis. BMC Cancer. 2009;9(1):11. https://doi.org/10.1186/1471-2407-9-11.
5. Ettinger KS, Ganry L, Fernandes RP. Oral cavity cancer. Oral Maxillofac Surg Clin N Am. 2019;31(1):13–29. https://doi.org/10.1016/j.coms.2018.08.002.
6. Greenberg JS, El Naggar AK, Mo V, et al. Disparity in pathologic and clinical lymph node staging in oral tongue carcinoma: implications for therapeutic decision making. Cancer. 2003;98(3):508–15. https://doi.org/10.1002/cncr.11526.
7. Han D, Liu J, Chen C, et al. Anti-tumour immunity controlled through mRNA m(6)A methylation and YTHDF1 in dendritic cells. Nature. 2019;566(7743):270–4. https://doi.org/10.1038/s41586-019-0916-x.
8. Howard A, Agrawal N, Gooi Z. Lip and oral cavity squamous cell carcinoma. Hematol Oncol Clin N Am. 2021;35(5):895–911. https://doi.org/10.1016/j.hoc.2021.05.003.
9. Hu Q, Peng J, Chen X, et al. Obesity and genes related to lipid metabolism predict poor survival in oral squamous cell carcinoma. Oral Oncol. 2019;89:14–22. https://doi.org/10.1016/j.oraloncology.2018.12.006.
10. Huang CF, Yu GT, Wang WM, et al. Prognostic and Predictive Values of SPP1, PAI and Caveolin-1 in Patients with Oral Squamous Cell Carcinoma. Int J Clin Exp Pathol. 2014;7(9):6032–9.
11. Huang DW, Sherman BT, Lempicki RA. Systematic and integrative analysis of large gene lists using DAVID bioinformatics resources. Nat Protoc. 2009;4(1):44–57. https://doi.org/10.1038/nprot.2008.211.
12. Huang L, Song F, Sun H, et al. IRX 5 promotes NF-κB signalling to increase proliferation, migration and invasion via OPN in tongue squamous cell carcinoma. J Cell Mol Med. 2018;22(8):3899–910. https://doi.org/10.1111/jcmm.13664.
13. Jin Y, Chen J, Feng Z, et al. OPN and $\mathbf{A}\nu\beta3$ expression are predictors of disease severity and worse prognosis in hepatocellular carcinoma. PLoS ONE. 2014;9(2): e87930. https://doi.org/10.1371/journal.pone.0087930.
14. Kale S, Raja R, Thorat D, et al. Osteopontin signaling upregulates cyclooxygenase-2 expression in tumor-associated macrophages leading to enhanced angiogenesis and melanoma growth via $\mathbf{A}9\beta1$ integrin. Oncogene. 2014;33(18):2295–306. https://doi.org/10.1038/onc.2013.184.
15. Karn T, Jiang T, Hatzis C, et al. Association between genomic metrics and immune infiltration in triple-negative breast cancer. JAMA Oncol. 2017;3(12):1707. https://doi.org/10.1001/jamaoncol.2017.2140.
16. Kim Y-J, Kim JH. Increasing incidence and improving survival of oral tongue squamous cell carcinoma. Sci Rep. 2020;10(1):7877. https://doi.org/10.1038/s41598-020-64748-0.
17. Liu K, Hu H, Jiang H, et al. RUNX1 promotes MAPK signaling to increase tumor progression and metastasis via OPN in head and neck cancer. Carcinogenesis. 2021;42(3):414–22. https://doi.org/10.1093/carcin/bgaa116.
18. Liu X, Wu S, Yang Y, et al. The prognostic landscape of tumor-infiltrating immune cell and immunomodulators in lung cancer. Biomed Pharmacother. 2017;95:55–61. https://doi.org/10.1016/j.biopha.2017.08.003.
19. McAllister SS, Gifford AM, Greiner AL, et al. Systemic endocrine instigation of indolent tumor growth requires osteopontin. Cell. 2008;133(6):994–1005. https://doi.org/10.1016/j.cell.2008.04.045.
20. McAllister SS, Weinberg RA. Tumor–host interactions: a far-reaching relationship. J Clin Oncol. 2010;28(26):4022–8. https://doi.org/10.1200/JCO.2010.28.4257.
21. Mei J, Xiao Z, Guo C, et al. Prognostic impact of tumor-associated macrophage infiltration in non-small cell lung cancer: a systemic review and meta-analysis. Oncotarget. 2016;7(23):34217–28. https://doi.org/10.18632/oncotarget.9079.
22. Montero PH, Patel SG. Cancer of the oral cavity. Surg Oncol Clin N Am. 2015;24(3):491–508. https://doi.org/10.1016/j.soc.2015.03.006.
23. Moorman HR, Poschel D, Klement JD, et al. Osteopontin: a key regulator of tumor progression and immunomodulation. Cancers. 2020;12(11):3379. https://doi.org/10.3390/cancers12113379.
24. Nallasamy P, Nimmakayala RK, Karmakar S, et al. Pancreatic tumor microenvironment factor promotes cancer stemness via SPP1–CD44 axis. Gastroenterology. 2021;161(6):1998-2013.e7. https://doi.org/10.1053/j.gastro.2021.08.023.
25. Naruse T, Yanamoto S, Okuyama K, et al. Immunohistochemical study of PD-1/PD-L1 axis expression in oral tongue squamous cell carcinomas: effect of neoadjuvant chemotherapy on local recurrence. Pathol Oncol Res. 2020;26(2):735–42. https://doi.org/10.1007/s12253-019-00606-3.
26. Nibu K, Hayashi R, Asakage T, et al. Japanese clinical practice guideline for head and neck cancer. Auris Nasus Larynx. 2017;44(4):375–80. https://doi.org/10.1016/j.anl.2017.02.004.
27. Pan Y, Yu Y, Wang X, et al. Tumor-associated macrophages in tumor immunity. Front Immunol. 2020;11: 583084. https://doi.org/10.3389/fimmu.2020.583084.
28. Peraramelli S, Zhou Q, Zhou Q, et al. Thrombin cleavage of osteopontin initiates osteopontin's tumor-promoting activity. J Thromb Haemost. 2022;20(5):1256–70. https://doi.org/10.1111/jth.15663.
29. Raineri D, Dianzani C, Cappellano G, et al. Osteopontin binds ICOSL promoting tumor metastasis. Commun Biol. 2020;3(1):615. https://doi.org/10.1038/s42003-020-01333-1.
30. Rangaswami H, Bulbule A, Kundu GC. Osteopontin: role in cell signaling and cancer progression. Trends Cell Biol. 2006;16(2):79–87. https://doi.org/10.1016/j.tcb.2005.12.005.
31. Rao G, Wang H, Li B, et al. Reciprocal interactions between tumor-associated macrophages and CD44-positive cancer cells via osteopontin/CD44 promote tumorigenicity in colorectal cancer. Clin Cancer Res. 2013;19(4):785–97. https://doi.org/10.1158/1078-0432.CCR-12-2788.
32. Reis PP, Waldron L, Perez-Ordonez B, et al. A gene signature in histologically normal surgical margins is predictive of oral carcinoma recurrence. BMC Cancer. 2011;11(1):437. https://doi.org/10.1186/1471-2407-11-437.
33. Rentoft M, Coates PJ, Laurell G, et al. Transcriptional profiling of formalin fixed paraffin embedded tissue: pitfalls and recommendations for

identifying biologically relevant changes. PLoS ONE. 2012;7(4): e35276. https://doi.org/10.1371/journal.pone.0035276.
34. Sun Y, Wu L, Zhong Y, et al. Single-cell landscape of the ecosystem in early-relapse hepatocellular carcinoma. Cell. 2021;184(2):404-421.e16. https://doi.org/10.1016/j.cell.2020.11.041.
35. Szklarczyk D, Franceschini A, Wyder S, et al. STRING V10: protein–protein interaction networks, integrated over the tree of life. Nucleic Acids Res. 2015;43(D1):D447–52. https://doi.org/10.1093/nar/gku1003.
36. Vitale I, Manic G, Coussens LM, et al. Macrophages and metabolism in the tumor microenvironment. Cell Metab. 2019;30(1):36–50. https://doi.org/10.1016/j.cmet.2019.06.001.
37. Wei J, Marisetty A, Schrand B, et al. Osteopontin mediates glioblastoma-associated macrophage infiltration and is a potential therapeutic target. J Clin Invest. 2018;129(1):137–49. https://doi.org/10.1172/JCI121266.
38. Xu X-L, Liu H, Zhang Y, et al. SPP1 and FN1 are significant gene biomarkers of tongue squamous cell carcinoma. Oncol Lett. 2021;22(4):713. https://doi.org/10.3892/ol.2021.12974.
39. Yang S, Wei J, Cui YH, et al. m(6)A mRNA demethylase FTO regulates melanoma tumorigenicity and response to anti-PD-1 blockade. Nat Commun. 2019;10(1):2782. https://doi.org/10.1038/s41467-019-10669-0.
40. Yuan Z-Y, Luo R-Z, Peng R-J, et al. High infiltration of tumor-associated macrophages in triple-negative breast cancer is associated with a higher risk of distant metastasis. OncoTargets Ther. 2014;7:1475. https://doi.org/10.2147/OTT.S61838.
41. Zhang H, Guo M, Chen J, et al. Osteopontin knockdown inhibits $a_v\beta_3$ integrin-induced cell migration and invasion and promotes apoptosis of breast cancer cells by inducing autophagy and inactivating the PI3K/Akt/mTOR pathway. Cell Physiol Biochem. 2014;33(4):991–1002.
42. Zhang X, Zhang L, Tan X, et al. Systematic analysis of genes involved in oral cancer metastasis to lymph nodes. Cell Mol Biol Lett. 2018;23(1):53. https://doi.org/10.1186/s11658-018-0120-2.
43. Zhang X, Zhang S, Yan X, et al. m6A regulator-mediated RNA methylation modification patterns are involved in immune microenvironment regulation of periodontitis. J Cell Mol Med. 2021;25(7):3634–45. https://doi.org/10.1111/jcmm.16469.
44. Zhou R, Zhang J, Zeng D, et al. Immune cell infiltration as a biomarker for the diagnosis and prognosis of stage I–III colon cancer. Cancer Immunol Immunother. 2019;68(3):433–42. https://doi.org/10.1007/s00262-018-2289-7.
45. Zhu Y, Yang J, Xu D, et al. Disruption of tumour-associated macrophage trafficking by the osteopontin-induced colony-stimulating factor-1 signalling sensitises hepatocellular carcinoma to anti-PD-L1 blockade. Gut. 2019;68(9):1653–66. https://doi.org/10.1136/gutjnl-2019-318419.
46. Zou B, Li J, Xu K, et al. Identification of key candidate genes and pathways in oral squamous cell carcinoma by integrated bioinformatics analysis. Exp Ther Med. 2019. https://doi.org/10.3892/etm.2019.7442.

Publisher's Note